analytical chemistry

ARTICLE

pubs.acs.org/ac

Photothermal Nanoblade for Large Cargo Delivery into Mammalian Cells

Ting-Hsiang Wu,[†] Tara Teslaa,[‡] Sheraz Kalim,[‡] Christopher T. French,[§] Shahriar Moghadam,[§] Randolph Wall,[§,∥,⊥] Jeffery F. Miller,[§,⊥,⊗] Owen N. Witte,[§,∥,⊥,⊗,○,#] Michael A. Teitell,[*,‡,∥,⊥,⊗] and Pei-Yu Chiou[*,⊗,▽]

[†]Department of Electrical Engineering, University of California, Los Angeles (UCLA), 420 Westwood Plaza, 43-147, Los Angeles, California 90095, United States

[‡]Department of Pathology and Laboratory Medicine, UCLA, 675 Charles E. Young Dr. South, MRL 4-762, Los Angeles, California 90095, United States

[§]Department of Microbiology, Immunology and Molecular Genetics, UCLA, 615 Charles E. Young Drive South, Los Angeles, California 90095, United States

[∥]Broad Center of Regenerative Medicine and Stem Cell Research, UCLA, 615 Charles E. Young Drive South, Los Angeles, California 90095, United States

[⊥]Molecular Biology Institute, UCLA, 611 Charles E. Young Drive East, Box 951570, Los Angeles, California 90095-1570, United States

[⊗]California NanoSystems Institute, UCLA, 570 Westwood Plaza Building 114, Los Angeles, California 90095, United States

[○]Molecular and Medical Pharmacology, UCLA, 675 Charles E. Young Drive South, MRL 5-748, Los Angeles, California 90095, United States

[#]Howard Hughes Medical Institute, 4000 Jones Bridge Road, Chevy Chase, Maryland 20815-6789, United States

[▽]Department of Mechanical and Aerospace Engineering, UCLA, 420 Westwood Plaza, 37-138, Los Angeles, California 90095, United States

Supporting Information

ABSTRACT: It is difficult to achieve controlled cutting of elastic, mechanically fragile, and rapidly resealing mammalian cell membranes. Here, we report a photothermal nanoblade that utilizes a metallic nanostructure to harvest short laser pulse energy and convert it into a highly localized explosive vapor bubble, which rapidly punctures a lightly contacting cell membrane via high-speed fluidic flows and induced transient shear stress. The cavitation bubble pattern is controlled by the metallic structure configuration and laser pulse duration and energy. Integration of the metallic nanostructure with a micropipet, the nanoblade generates a micrometer-sized membrane access port for delivering highly concentrated cargo (5×10^8 live bacteria/mL) with high efficiency (46%) and cell viability (>90%) into mammalian cells. Additional biologic and inanimate cargo over 3-orders of magnitude in size including DNA, RNA, 200 nm polystyrene beads, to 2 μm bacteria have also been delivered into multiple mammalian cell types. Overall, the photothermal nanoblade is a new approach for delivering difficult cargo into mammalian cells.

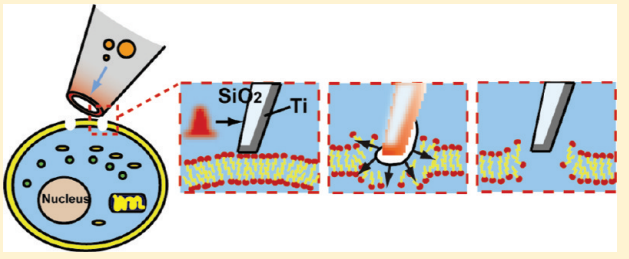

Transferring cargo into mammalian cells over a wide range of sizes, including proteins, DNA, RNA, chromosomes, nuclei, and inanimate particles, such as quantum dots, surface-enhanced Raman scattering (SERS) particles, and microbeads, is highly desirable in many fields of biology. Delivery methods, such as endocytosis, can entrap cargo in an endosome, where the low pH microenvironment and lytic enzymes often lead to cargo degradation.[1] Viral and chemical delivery methods package the cargo inside a virus or form chemical complexes that enhance uptake.[2,3] However, toxicity, cell-type specific uptake, and more importantly limited cargo packing capacity impose a significant constraint on cargo size and transferable cell types.[1] Physical transfer methods include electroporation[4] and sonoporation,[5] which produce randomly distributed nanoscale pores, and optoporation,[6−8] which generates pores on the cell membrane at the laser focal point. Through these pores, small cargo is delivered into cells by thermal diffusion or by an electric field. Delivery of large cargo with these methods has low efficiency due to the slow speed of cargo diffusion and decreasing cell viability with increasing pore size.[9] Microcapillary injection[10,11] uses a sharp

Received: September 24, 2010
Accepted: December 23, 2010
Published: January 19, 2011

glass tip to mechanically penetrate a cell membrane for delivery. However, mechanical trauma from membrane penetration limits the typical pipet tip to 0.5 μm in diameter in order to maintain cell viability.[11,12] Cargo larger than the pipet tip cannot be injected due to pipet clogging and cargo shearing. Electroinjection, which combines electroporation with microcapillary injection, has demonstrated small molecule delivery, such as RNA and plasmid DNA, into live cells[13,14] and bacteria delivery into artificial lipid vesicles[15] by weakening the contacting cell membrane with an electric field, followed by gentle mechanical penetration into the cell. However, methods for high efficiency delivery of micrometer-sized cargo into live mammalian cells have yet to be achieved. Alternatively, a simple lipid assisted microinjection (SLAM) technique[16] incorporates synthetic lipid molecules at the tip of a glass microcapillary. Contact of the SLAM micropipet with a cell membrane allowed the lipid molecules to fuse with the cell membrane to form a continuous and temporary pathway for cargo delivery. This method avoids the zigzag stabbing motion of the micropipet tip through the cell membrane. However, the lipohilic interactions with cargo and cell membrane could produce unwanted biological effects in the cell as well as with the delivery cargo, limiting this method to specific cell types and cargo contents. One of the major technical barriers is the lack of an ability to open large access ports in cell membranes with minimal damage to mechanically fragile, elastic, and three-dimensional cell membranes.

Collective electron oscillations on metallic nanostructures, known as surface plasmons, have intriguing optical properties and have been utilized to demonstrate novel optical applications including optical cloaking,[17] superlensing,[18] near-field imaging,[19] and SERS detection.[20] With control of the three-dimensional configuration of such structures, specific resonance frequencies and optical absorption properties can be designed.[21] The kinetic energy of oscillating electrons driven by applied electromagnetic fields is converted into lattice heat in picoseconds,[22] which heats up the surrounding medium through thermal conduction. Such metallic nanostructure-guided photothermal effects have been shown to guide nanowire growth,[23] actuate micro- and nanoscale fluids,[24,25] provide photothermal cancer therapy,[26,27] and trigger drug delivery.[28,29] An interesting phenomenon occurs when a metallic nanostructure is immersed in aqueous media and heated rapidly with a short laser pulse. A substantial temperature rise is realized in the nanostructure and in the thin surrounding liquid layer over the laser pulse duration. When a threshold energy is surpassed that superheats the liquid medium, part of the absorbed optical energy is converted into mechanical work through inducing explosive cavitation bubbles that generate localized and high speed fluid flows.[25,30] It has been demonstrated that gold nanospheres adhered to a mammalian cell membrane and exposed to nanosecond laser pulses generate randomly distributed nanoscale cavitation bubbles and transient membrane pores for small molecule delivery by diffusion or can cause membrane rupture and cell death if the induced cavitation bubbles are large.[27,31,32]

Here, we developed a photothermal nanoblade that is a metallic nanostructure integrated with a microcapillary pipet (Figure 1). The photothermal nanoblade harvests optical pulse energy to trigger spatially patterned, temporally synchronized cavitation bubbles that generate high-speed, localized fluidic flows. If a soft material or fragile structure, such as a cell membrane, is in contact with the photothermal nanoblade, the ultrafast and localized flow is able to puncture the membrane

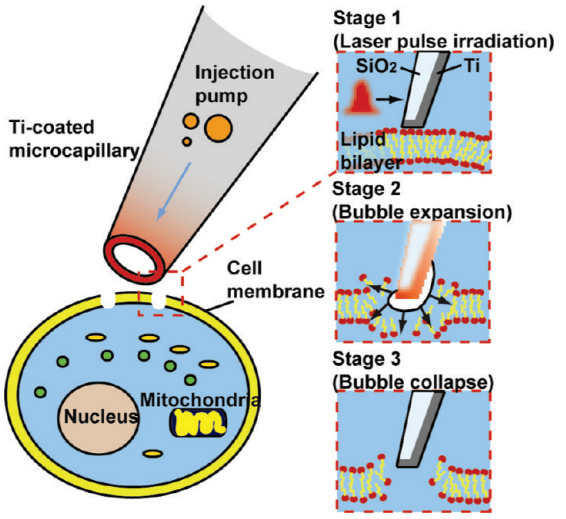

Figure 1. Ultrafast membrane cutting mechanism using a photothermal nanoblade for cargo delivery into live mammalian cells. A Ti thin film coats the outside of a glass micropipet. Upon excitation by a nanosecond laser pulse, the Ti heats rapidly, along with a thin surrounding aqueous layer through heat conduction. An explosive vapor nanobubble that expands and collapses in <1 μs locally cuts the contacting cell membrane in synchronization with pressure-driven delivery of the microcapillary contents.

near the contact area with little mechanical perturbation to the rest of the structure. Membrane cutting is produced by the strong transient mechanical shear stress from the laser-induced cavitation bubble.[33−35] A delivery portal in the cell membrane is thereby generated without advancing the attached micropipet into the cell. The blade is in gentle contact with the membrane during cutting, eliminating the need for strong mechanical support underneath the membrane. This new device allows intracellular delivery of variably sized objects, from biomolecules to bacteria, into soft mammalian somatic cells with high efficiency and cell viability.

To demonstrate the photothermal nanoblade, a 100 nm thick titanium (Ti) thin film was deposited onto the tip of a glass microcapillary pipet with a 2 μm tip diameter (Figure 2A,B). The Ti coated micropipet is mounted on a motorized micromanipulator arm on an inverted microscope stage. With the micropipet tip positioned in light contact with a cell membrane, a 6 ns Nd:YAG laser pulse at 532 nm wavelength illuminated a 260 μm-wide field through the objective lens. Pulsed laser exposure rapidly heats the Ti and adjacent thin water layer to induce a localized vapor bubble explosion along the ring-shaped Ti thin film that cuts the contacting cell membrane. The process, from laser pulsing, Ti heating, cavitation bubble expansion, and collapse, takes only a few hundred nanoseconds. Pressure-controlled delivery of fluid and cargo inside the micropipet is synchronized with laser pulsing and membrane cutting.

MATERIALS AND METHODS

Device Fabrication and Experimental Setup. Titanium (Ti)-coated micropipets were fabricated by heating and pulling (P-97, Sutter Instrument) a 1 mm diameter borosilicate glass capillary tube, followed by Ti thin film deposition onto the tapered ends using a magnetron sputter deposition system. The Ti coating thickness and the micropipet tip diameter were quantified using a scanning electron microscope. The laser pulse system was

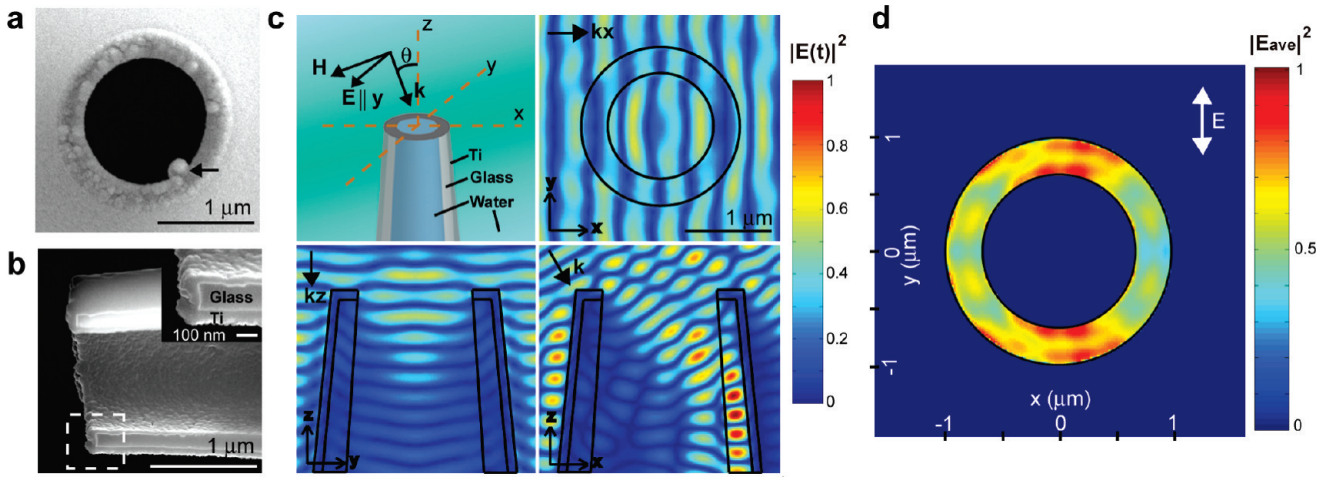

Figure 2. Structure of a Ti-coated micropipet and the calculated intensity pattern from laser excitation. (a,b) Scanning electron microscope images of a pulled, Ti-coated micropipet. Inner diameter = 1.38 ± 0.1 μm (mean ± s.d.). Outer diameter = 1.88 ± 0.1 μm. Thickness of Ti thin film = 102 ± 8 nm. (The arrow points to edge of the glass filament running inside the micropipet.) (c) Normalized intensity profiles at the tip of the micropipet under laser excitation ($n_{Ti} = 1.86 + 2.56i$,[36] $n_{glass} = 1.46$, $n_{water} = 1.34$, $\lambda = 532$ nm, $\theta = 30°$). (d) Time-averaged optical absorption profiles ($\propto |E_{ave}|^2$) in the Ti ring at the micropipet tip.

a Q-switched, frequency-doubled Nd:YAG laser (Minilite I, Continuum) operated at 532 nm wavelength and 6 ns pulsewidth. The laser beam was split by a polarizing beam splitter (Figure S-1 in the Supporting Information), with one arm sent into the fluorescence port of an inverted microscope (AxioObserver, Zeiss) and then through the objective lens (40×, 0.6 NA), to generate a 260 μm-wide laser spot on the sample plane. The optimized laser fluence used for cargo delivery was 180 mJ/cm^2 (Figure S-2 in the Supporting Information). An electrical switch was built to synchronize the excitation laser pulse with the liquid injection system (FemtoJet, Eppendorf). A time-resolved imaging system to characterize the cavitation bubble dynamics was constructed using an intensified CCD camera (PI-MAX2, Princeton Instruments) with exposure times as short as 500 ps. A programmable delay between receiving the laser triggering signal and the camera shutter opening was set by the camera control unit. After the polarizing beam splitter, the other arm of the laser beam was sent through a fluorescent dye cell. The excited fluorescence pulse (wavelength centered ~698 nm) was coupled into a multimode fiber and then sent through the microscope condenser to illuminate the sample in synchronization with the camera shutter. A nanosecond time delay between the captured bubble image and the sample excitation laser pulse was controlled by the length of the optical fiber delay line.

Numerical Calculations of Intensity Pattern on the Ti-Coated Micropipet. The 3D finite difference time domain (FDTD) method was used to simulate the electromagnetic intensity pattern (FullWAVE, RSoft Design Group). The simulation domain was constructed with a water medium region (n_{water}=1.34) and a glass micropipet (n_{glass} = 1.46) with a 100 nm Ti ($n_{Ti} = 1.86 + 2.56i$[36]) thin film coated on the tip and the outer sidewall. The entire domain was surrounded by perfectly matched boundary layers to mimic an infinitely extending space. Plane wave excitation was used (λ = 532 nm) with the electric field polarized along y and the wavevector k making a 30° angle with respect to the pipet tip. Time-averaged intensity profiles in Ti, $|E_{ave}|^2$, were obtained by averaging the normalized electric energy density over one electromagnetic wave oscillation.

Determining the Optimal Laser Fluence of the Photothermal Nanoblade for Membrane Cutting. Criteria for optimal laser fluence, membrane opening, and maintaining high cell viability were sought. Propidium iodide (PI) dye was added to the cell culture media (10 μg/mL) before laser pulsing. The micropipet was brought into contact with the cell membrane and illuminated with a laser pulse at the specified fluence level. The treated cell was checked immediately after laser pulsing to verify the uptake of PI. Cell viability was determined separately in a similar fashion with PI added 90 min after laser pulsing, followed by visual growth detection over time.

Cell Viability Evaluation. Cell viability was determined by annexin V and propidium iodide (PI) cell staining 90 min following photothermal nanoblade cutting. To accurately track injected cells, cells were seeded onto a chemically patterned glass coverslip substrate.[37] Circular areas (diameter ~200 μm) were defined on the substrate to confine cell adhesion and growth within these regions (Figure S-3 in the Supporting Information). For each experiment, every cell within the same circular pattern (~60 cells in one pattern) was subjected to the same laser pulsing and cargo delivery conditions. To exclude the viability effects of culturing cells on a patterned substrate, the percentage of viable cells in a treated pattern was further normalized by the percentage of viable cells in a neighboring untreated pattern on the same glass substrate. Postdelivery viability was determined by the average of three independent experiments.

Biomolecule, Carboxylate Bead, and Bacterial Delivery with Immunofluorescence Imaging. GFP-expressing RNA was diluted in 1× PBS, pH 7.4, and injected into IMR90 primary human lung fibroblasts. DsRed-encoding lentiviral DNA was incubated with cationic, 100 nm green polystyrene beads to allow DNA adsorption on the spherical surface. The beads were then suspended in 1× PBS, pH 7.4, and injected into human embryonic stem (hES) cells. hES cells were dissociated and cultured using ROCK[38] inhibitor on top of a thin layer of matrigel (BD Biosciences). DsRed expression was verified 24 h postinjection. Green carboxylate-modified polystyrene beads (200 nm) were suspended in 1× PBS, pH 7.4, (0.1% solid by volume) and injected into HEK293T cells. Fluorescent *B. thailandensis* bacteria

dx.doi.org/10.1021/ac102532w |*Anal. Chem.* 2011, 83, 1321–1327

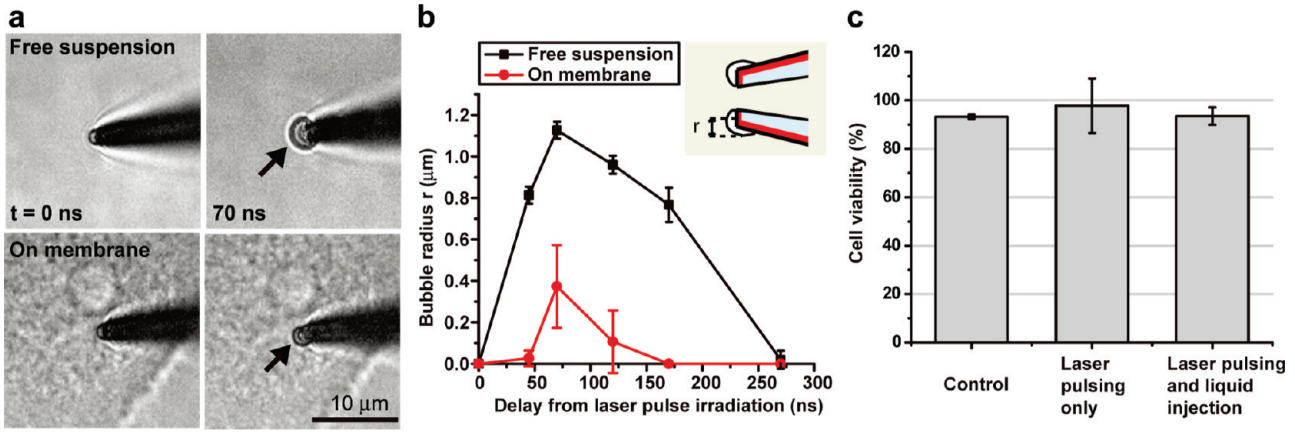

Figure 3. Ultrafast membrane cutting by the photothermal nanoblade and cell viability evaluation. (a) A nanobubble with maximum radius extending to 0.4 μm from the rim of the pipet tip when in contact with the cell membrane. Energy transfer to the contacting membrane reduces the size of nanobubble formation and locally cuts the plasma membrane. (b) Fast expansion and collapse dynamics of a vapor nanobubble within 270 ns in free suspension and 170 ns in contact with a HeLa cell membrane. (c) Cell viability postphotothermal delivery. The control experiment was performed using a glass-only micropipet in contact with the cell (no piercing through the membrane) and illuminating with a laser pulse at the same fluence (180 mJ/cm^2). Cell viability is >90% when cells were subjected to laser pulsing and membrane opening alone (98 ± 11% (mean ± s.d.)) and in experiments where cells were subjected to laser pulsing and liquid injection (94 ± 4%).

were suspended in 1× PBS, pH 7.4 (concentration 10^8-10^9 per mL) and injected into HeLa cells. Cells were cultured in chambered microscope slides (LabTek, Nunc) using Dulbecco's modified Eagle's medium (DMEM) without penicillin and streptomycin. Immediately after the injection, cells were washed 3 times with PBS and incubated for 2 h in fresh medium containing 1000 mg/mL kanamycin to kill extracellular bacteria. The growth medium was then replaced with DMEM containing 5 mg/mL ceftazidime to suppress extracellular bacterial growth and incubated for an additional 16−24 h at 37 °C in 5% CO_2. At 16−24 h postinjection, cells were fixed with 4% paraformaldehyde and stained with Alexa-Fluor-labeled phalloidin to visualize the actin cytoskeleton (Invitrogen). Cells were then visualized using a Leica SP2 AOBS laser scanning confocal microscope setup.

Bacterial Strains and Growth Conditions. *Burkholderia thailandensis* and mutant derivates were cultured in L-medium. Chloramphenicol (25 μg/mL) or tetracycline (20 μg/mL) were added as required.

Bacterial Invasion Efficiency Assays. *B. thailandensis* E264 was grown in L-broth to an optical density (OD_{600}) of 1.0 (4×10^8 CFU/mL). In total, 1×10^5 HeLa cells grown in 12-well plates were infected with bacteria at a multiplicity of infection (MOI) of 10:1 for 2 h at 37 °C. The infected cells were then washed with PBS and incubated with fresh medium containing 400 μg/mL kanamycin for 15 min to kill extracellular bacteria, followed by lysis with 1% Triton X-100 in PBS. Serial dilutions of the infected HeLa cell lysates were spread on L-agar, and the numbers of intracellular bacteria were determined by assays for CFU.

RESULTS AND DISCUSSION

Simulation of Optical Intensity Patterns on the Photothermal Nanoblade. The cavitation bubble pattern is controlled by the thin film composition and configuration, as well as laser excitation parameters including wavelength, pulse duration, and energy. Figure 2c shows the calculated intensity patterns on a laser-excited, Ti-coated micropipet using 3D finite difference time domain (FDTD) simulations. The Ti-coated micropipet is illuminated at an angle of 30° with respect to the tip. Plasmon-enhanced optical absorption ($\propto|E_{ave}|^2$) is nonuniform across a 2 μm wide Ti ring for linearly polarized light (Figure 2d). High intensity areas are concentrated on the edges of the rings along the wave polarization direction. The temperature distribution in the Ti ring is governed not only by the heat generated in these high intensity areas but also by heat diffusion to the cooler metal regions and surrounding medium during laser pulsing. In the Ti film on the micropipet, the estimated heat diffusion length ($\sim(D\tau)^{1/2}$) is 230 nm in 6 ns. This results in a smoother temperature profile along the entire ring-shaped pipet tip. Consequently, thermal energy conducting away from the Ti film heats the adjacent thin water layer to above the critical temperature,[25] generating a vapor nanobubble on the ring-shaped micropipet tip (Figure 3a).

Cavitation Bubble Induced Membrane Cutting and Corresponding Cell Viability. For micrometer-sized cargo delivery into live mammalian cells, a transient membrane portal must accommodate the cargo size. Moreover, the damage zone must also be contained to allow cell repair and maintain viability. Figure 3a shows cavitation bubbles at the tip of a tilted Ti-coated micropipet 70 ns after laser pulse irradiation. A dramatic reduction in the bubble size was observed when the tip was in contact with the cell membrane as this interaction impedes bubble expansion. In this case the bubble grew to a maximum radius of 400 nm away from the rim of the tip in 70 ns and collapsed completely within 200 ns after the excitation laser pulse (Figure 3a,b). The blade tip never enters the cell so intracellular structural integrity is preserved, which helps foster rapid, reparative pore resealing, as evidenced by sustained cell viability (Figure 3c). Cell viability was determined by annexin V and propidium iodide (PI) exclusion staining 90 min following laser pulsing. Under these conditions, >90% cell viability was obtained with laser pulsing and bubble explosion alone (at an optimal fluence of 180 mJ/cm^2, Figure S-2 in the Supporting Information) or when coupled with buffer injection into HeLa or HEK293T cells. Monitoring photothermal nanoblade treated cells over 24 h showed that cells stayed viable and continued

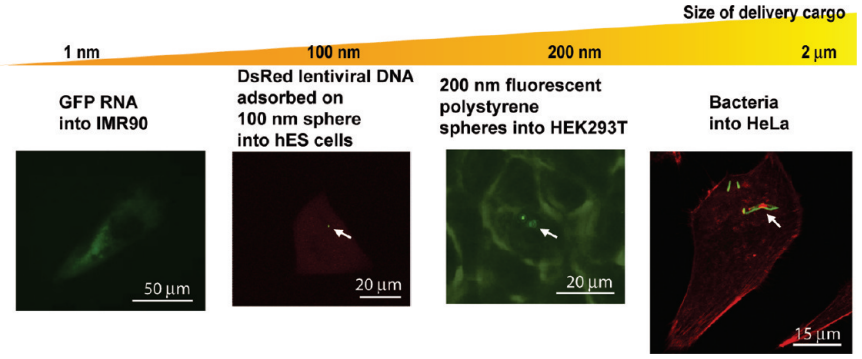

Figure 4. Wide range of deliverable cargo sizes by the photothermal nanoblade. GFP-expressing RNA was delivered into lipofectamine-resistant IMR90 primary human lung fibroblasts. DsRed-containing lentivirus coated onto a 100 nm green fluorescent bead was expressed in ROCK inhibitor dispersed human embryonic stem cells following transfer. Fluorescent beads of 200 nm in diameter were delivered into HEK293T cells without clogging. *B. thailandensis* bacterial transfer into HeLa cells was achieved with high efficiency and high cell viability.

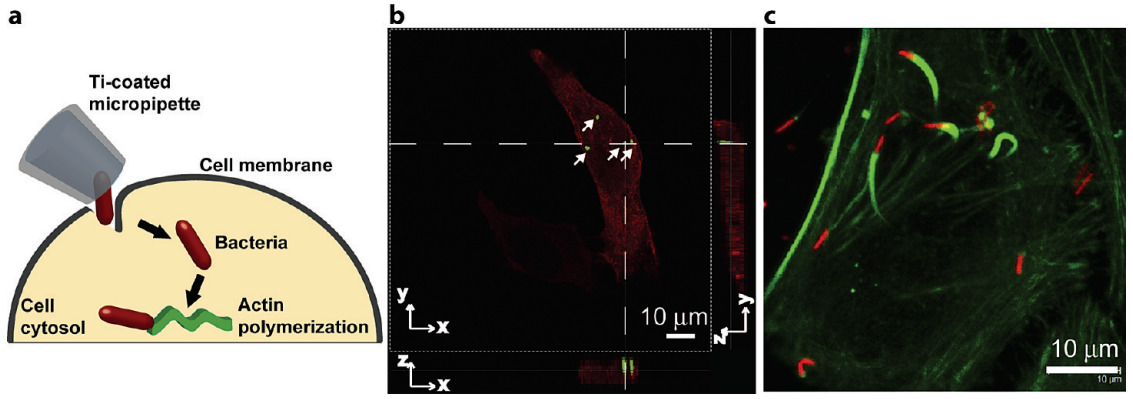

Figure 5. High-efficiency bacterial delivery into HeLa cells by the phothermal nanoblade. (a) Pathway of bacterial uptake following transfer.[39] (b) GFP-labeled *Burkholderia thailandensis* was transferred into a HeLa cell (average efficiency = 46 ± 33% (mean ± s.d.)) along with red-fluorescent dextran-tetramethylrhodamine. Confocal *z*-axis scanning showing multiple bacteria inside a red-fluorescent cell. (c) Multiplication and actin polymerization of transferred mCherry-labeled *B. thailandensis* in HeLa cells.

to grow and divide as usual (Figure S-3 in the Supporting Information).

Biomolecules and Bacteria Delivery by the Photothermal Nanoblade. We tested the delivered cargo size range using the photothermal nanoblade on various cell types. GFP-expressing RNA was efficiently delivered into lipofectamine-resistant IMR90 primary human lung fibroblasts, and a DsRed-containing lentivirus coated onto 100 nm green fluorescent polystyrene beads was successfully expressed in ROCK[38] inhibitor dispersed human embryonic stem cells following injection. Fluorescent beads of 200 nm in diameter were delivered without clogging, as were micrometer-sized bacteria (Figure 4). We further evaluated an intracellular bacterium as the largest and most fragile cargo delivered by this approach (Figure 5). *Burkholderia thailandensis*[39] is a rod-shaped bacteria measuring ~0.7 μm × 2 μm. To determine injection efficiency, GFP-labeled bacteria were suspended in buffer at a concentration of ~5×10^8 per mL, 2 orders of magnitude higher than conventional microinjection.[40] High cargo concentration is critical in achieving high delivery efficiency since the liquid volume delivered into a cell is limited to ~1 pL. Without a high concentration, the frequency of ejecting 1 bacterium per injection is low. In our experiment, upon laser pulsing and cell membrane opening, 1−5 pL of the bacterial solution was ejected out of the pipet, corresponding to an average of ~1 bacteria per injection. Not all the ejected solution was delivered into the cell since the pipet tip was in light contact with the cell membrane, and the bore of the pipet was not in a perfect seal with the membrane after cutting. Under this condition, we obtained an average delivery efficiency of 46% from multiple independent experiments (Table S-1 in the Supporting Information). We further evaluated the natural bacterial invasion efficiency in HeLa cells by incubating cells with *B. thailandensis* for 2 h. The delivery efficiency by photothermal injection is 2 orders of magnitude higher than the natural HeLa cell infectivity of *B. thailandensis* of 0.8%. Importantly, bacteria remained viable and were protected from destruction during bubble cycles within the glass pipet and from shearing during injection by the large bore tip opening as verified by bacteria multiplication and actin polymerization[41] in the injected cells 24 h after transfer (Figure 5c).

Reliability Evalution of the Photothermal Nanoblade. For robust operation, the metallic thin film must withstand high temperature and intense pressure from the shockwave and high-speed flows generated by cavitation bubbles. Ti was chosen as the coating material for its higher melting temperature and strong adhesion to the glass substrate compared with other inert metals such as gold.[42] It has been shown in our experiments that a gold-coated micropipet failed after a few laser pulses due to thin film

damage. We verified that a Ti-coated micropipet remained functional through at least 50 laser pulsing and bubble explosion cycles. (Figure S-4 in the Supporting Information).

CONCLUSIONS

The photothermal nanoblade holds promise for delivering currently untransferable large cargo into mammalian cells, such as chromosomes, organelles, and intracellular pathogens, that are beyond the size constraints of contemporary delivery approaches. An additional advantage of the photothermal nanoblade is its ease of use. Since membrane cutting is controlled by the laser pulse energy and the Ti coating configuration, the user simply positions the micropipet tip in gentle contact with the cell membrane to perform delivery. By contrast, for conventional glass microcapillary microinjection, delivery efficiency and cell viability are strongly influenced by the manner in which the glass needle enters the cell (e.g., speed, force, angle). As a result, the conventional method requires substantial training and experience for a user to become proficient. There is also less chance to break the fragile micropipet tip using the photothermal nanoblade since it does not require a rapid "zig-zag" motion for the micropipet to penetrate and leave the cell. The photothermal nanoblade does not operate under any specific surface plasmon resonance modes in the current demonstration. Further optimization of the metallic nanostructure to match the excitation laser wavelength could reduce the threshold laser energy for exciting cavitation bubbles.

ASSOCIATED CONTENT

Supporting Information. Additional information as noted in text. This material is available free of charge via the Internet at http://pubs.acs.org.

AUTHOR INFORMATION

Corresponding Author

*Michael A. Teitell: e-mail, mteitell@ucla.edu; address, 675 Charles E. Young Dr. South, MRL 4-762, Los Angeles, CA 90095; phone, (310) 206-6754; fax, (310) 267-0382. Pei-Yu Chiou: e-mail, pychiou@seas.ucla.edu; address, 420 Westwood Plaza, 37-138, Los Angeles, CA 90095; phone, (310) 825-8620; fax, (310) 206-4830.

ACKNOWLEDGMENT

M.A.T. and P.-Y.C. are co-contributing authors. The authors thank Dr. Kayvan Niazi and Dr. Shahrooz Rabizadeh (California NanoSystems Institute and Abraxis BioScience) for helpful discussions and support. We gratefully thank Isla P. Garraway, Rita U. Lukacs, Eric H. Gschweng, Xinqiang Huang, and Jennifer Anderson for exceptional technical support and the CNSI Advanced Light Microscopy and Spectroscopy Facility at UCLA, which is supported by an NIH-NCRR shared resources grant (Grant CJX1-443835-WS-29646) and NSF Major Research Instrumentation grant (Grant CHE-0722519). This project is supported by the NSF (Grants CBET 0853500 and ECCS 0901154), a UC Discovery/Abraxis BioScience Biotechnology Award (Grant No. 178517), the NIH Roadmap for Medical Research Nanomedicine Initiative (Grant PN2EY018228), the Broad Center of Regenerative Medicine and Stem Cell Research at UCLA, the Prostate Cancer Foundation Challenge Award, and the Pacific Southwest Regional Center of Excellence in Biodefense and Emerging Infectious Diseases (Grant U54 AI065359).

REFERENCES

(1) Luo, D.; Saltzman, W. M. *Nat. Biotechnol.* **2000**, *18*, 33–37.
(2) Naldini, L.; Blomer, U.; Gallay, P.; Ory, D.; Mulligan, R.; Gage, F. H.; Verma, I. M.; Trono, D. *Science* **1996**, *272*, 263–267.
(3) Felgner, P. L.; Gadek, T. R.; Holm, M.; Roman, R.; Chan, H. W.; Wenz, M.; Northrop, J. P.; Ringold, G. M.; Danielsen, M. *Proc. Natl. Acad. Sci. U.S.A.* **1987**, *84*, 7413–7417.
(4) Chu, G.; Hayakawa, H.; Berg, P. *Nucleic Acids Res.* **1987**, *15*, 1311–1326.
(5) Mitragotri, S. *Nat. Rev. Drug Discovery* **2005**, *4*, 255–260.
(6) Tirlapur, U. K.; König, K. *Nature* **2002**, *418*, 290–291.
(7) Vogel, A.; Noack, J.; Hűttman, G.; Paltauf, G. *Appl. Phys. B: Laser Opt.* **2005**, *81*, 1015–1047.
(8) Clark, I. B.; Hanania, E. G.; Stevens, J.; Gallina, M.; Fieck, A.; Brandes, R.; Palsson, B. O.; Koller, M. R. *J. Biomed. Opt.* **2006**, *11*, 014034.
(9) Stevenson, D.; Agate, B.; Tsampoula, X.; Fischer, P.; Brown, C. T. A.; Sibbett, W.; Riches, A.; Gunn-Moore, F.; Dholakia, K. *Opt. Express* **2006**, *14*, 7125–7133.
(10) King, R. *Gene delivery to mammalian cells by microinjection. Methods in Molecular Biology 245: Gene Delivery to Mammalian Cells 1*; Humana Press Inc.: Totowa, NJ, 2004.
(11) Zhang, Y. *Nat. Protoc.* http://www.natureprotocols.com/2007/11/02/microinjection_technique_and_p.php, published online November 2, **2007**.
(12) Han, S.-W.; Nakamura, C.; Kotobuki, N.; Obataya, I.; Ohgushi, H.; Nagamune, T.; Miyake, J. *Nanomed. Nanotechnol. Biol. Med.* **2008**, *4*, 215–225.
(13) Boudes, M.; Pieraut, S.; Valmier, J.; Carroll, P.; Scamps, F. *J. Neurosci. Methods* **2008**, *170*, 204–211.
(14) Kitamura, K.; Judkewitz, B.; Kano, M.; Denk, W.; Häusser, M. *Nat. Methods* **2008**, *5*, 61–67.
(15) Hurtig, J.; Orwar, O. *Soft Matter* **2008**, *4*, 1515–1520.
(16) Laffafian, I.; Hallett, M. B. *Biophys. J.* **1998**, *75*, 2558–2563.
(17) Kildishev, A. V.; Shalaev, V. M. *Nat. Photonics* **2007**, *1*, 224–227.
(18) Fang, N.; Lee, H.; Sun, C.; Zhang, X. *Science* **2005**, *308*, 534–537.
(19) Betzig, E.; Trautman, J. K. *Science* **1992**, *257*, 189–195.
(20) Nie, S.; Emory, S. R. *Science* **1997**, *21*, 1102–1106.
(21) Prodan, E.; Radloff, C.; Halas, N. J.; Nordlander, P. *Science* **2003**, *302*, 419–422.
(22) Link, S.; El-Sayed, M. A. *J. Phys. Chem. B* **1999**, *103*, 8410–8426.
(23) Cao, L.; Barsic, D. N.; Guichard, A. R.; Brongersma, M. L. *Nano Lett.* **2007**, *7*, 3523–3527.
(24) Liu, G. L.; Kim, J.; Lu, Y.; Lee, L. P. *Nat. Mater.* **2005**, *5*, 27–32.
(25) Kotaidis, V.; Dahmen, C.; von Plessen, G.; Springer, F.; Plech, A. *J. Chem. Phys.* **2006**, *124*, 184702.
(26) Jain, P. K.; El-Sayed, I. H.; El-Sayed, M. A. *Nano Today* **2007**, *2*, 18–29.
(27) Lapotko, D. O.; Lukianova, E.; Oraevsky, A. A. *Laser Surg. Med.* **2006**, *38*, 631–642.
(28) Skirtach, A. G.; Dejugnat, C.; Braun, D.; Susha, A. S.; Rogach, A. L.; Parak, W. J.; Mohwald, H.; Sukhorukov, G. B. *Nano Lett.* **2005**, *5*, 1371–1377.
(29) Lee, S. E.; Liu, G. L.; Kim, F.; Lee, L. P. *Nano Lett.* **2009**, *9*, 562–570.
(30) Lukianova-Hleb, E.; Hu, Y.; Latterini, L.; Tarpani, L.; Lee, S.; Drezek, R. A.; Hafner, J. H.; Lapotko, D. O. *ACS Nano* **2010**, *4*, 2109–2123.
(31) Pitsillides, C. M.; Joe, E. K.; Wei, X. B.; Anderson, R. R.; Lin, C. P. *Biophys. J.* **2003**, *84*, 4023–4032.
(32) Wu, T.-H.; Kalim, S.; Callahan, C.; Teitell, M. A.; Chiou, P.-Y. *Opt. Express* **2010**, *18*, 938–946.
(33) Marmottant, P.; Hilgenfeldt, S. *Nature* **2003**, *423*, 153–156.

(34) Lokhandwalla, M.; Sturtevant, B. *Phys. Med. Biol.* **2001**, *46*, 413–437.
(35) Hellman, A.; Rau, K. R.; Yoon, H. H.; Venugopalan, V. *J. Biophoton.* **2008**, *1*, 24–35.
(36) Lynch, D. W.; Hunter, W. R. Introduction to the data for several metals. In *Handbook of Optical Constants of Solids* , Vol. III; Academic Press: San Diego, CA, 1998.
(37) Peterbauer, T.; Heitz, J.; Olbrich, M.; Hering, S. *Lab Chip* **2006**, *6*, 857–863.
(38) Watanabe, K.; Ueno, M.; Kamiya, D.; Nishiyama, A.; Matsumura, M.; Wataya, T.; Takahashi, J. B.; Nishikawa, S.; Nishikawa, S.-I.; Muguruma, K.; Sasai, Y. *Nat. Biotechnol.* **2007**, *25*, 681–686.
(39) Wiersinga, W. J.; van der Poll, T.; White, N. J.; Day, N. P.; Peacock, S. J. *Nat. Rev. Microbiol.* **2006**, *4*, 272–282.
(40) Goetz, M.; Bubert, A.; Wang, G.; Chico-Calero, I.; Vazquez-Boland, J.; Beck, M.; Slaghuis, J.; Szalay, A. A.; Goebel, W. *Proc. Natl. Acad. Sci. U.S.A.* **2001**, *98*, 12221–12226.
(41) Stevens, J. M.; Ulrich, R. L.; Taylor, L. A.; Wood, M. W.; DeShazer, D.; Stevens, M. P.; Galyov, E. E. *J. Bacteriol.* **2005**, *187*, 7857–7862.
(42) Benjamin, P.; Weaver, C. *Proc. R. Soc. London, Ser. A* **1961**, *261*, 516–531.